Crystal chemistry and ion conductivity of the Na$_{1+x}$Ti$_{2-x}$Al$_x$(PO$_4$)$_3$ (0 ≤ x ≤ 0.9) NASICON series

F. E. Mouahid,[a] M. Bettach,[a] M. Zahir,[a] P. Maldonado-Manso,[b] S. Bruque,*[b] E. R. Losilla[b] and M. A. G. Aranda[b]

[a]L.P.C.M. Département de Chimie, Faculté des Sciences, Université Chouaib Doukkali, El Jadida 24000, Morocco

[b]Departamento de Química Inorgánica, Cristalografía y Mineralogía, Universidad de Málaga, 29071 Málaga, Spain. E-mail: bruque@uma.es

The Na$_{1+x}$Ti$_{2-x}$Al$_x$(PO$_4$)$_3$ (0.0 ≤ x ≤ 0.9) solid solution has been prepared as a polycrystalline powder. These compounds crystallise in the NASICON type structure, $R\bar{3}c$ space group, and the crystal structures have been characterised by the Rietveld method with laboratory powder diffraction data. The Ti/Al atoms are randomly distributed over the octahedral site of the NASICON framework. The negatively charged framework is neutralised by the Na$^+$ cations which are distributed over the M1 site, fully occupied, and M2 site, partly occupied. The cell parameter evolution along the series agrees with the substitution of larger Ti^{4+} by smaller Al^{3+} cations. The thermal expansion coefficients were determined from a thermodiffractometric study of Na$_{1.8}$Ti$_{1.2}$Al$_{0.8}$(PO$_4$)$_3$. The ion conductivity of the samples rises as the charge carrier number (x) increases. The activation energies deduced from the Arrhenius plots are close to 0.50 eV. The overall conductivities are near to 10^{-5} S cm^{-1} at 200 °C.

Introduction

The original "**Na s**uper **i**onic **con**ductors" NASICON materials were solid solutions derived from NaZr$_2$P$_3$O$_{12}$ by partial replacement of P by Si with extra Na to balance the charges. The resulting general formula is Na$_{1+x}$Zr$_2$P$_{3-x}$Si$_x$O$_{12}$ (0 ≤ x ≤ 3).[1,2] Since then, a large number of related materials has been synthesised, mainly phosphates. Related phosphate series are those obtained by partial substitution of tetravalent M^{IV} cations by trivalent M^{III} ones to yield Na$_{1+x}$M$^{IV}_{2-x}$M$^{III}_x$(PO$_4$)$_3$. The compositional limit, x_{max}, depends on the nature and ionic radii of the octahedral cations.[3–8] These compounds have been extensively studied because of the high conductivity shown by some compositions. They are versatile materials and can tolerate a wide range of compositional variation.

The NASICON structure has a negatively charged 3D-framework, of general formula M$_2$X$_3$O$_{12}$, within which the Na$^+$ cations reside in fully or partially occupied sites. The framework is built of XO$_4$ tetrahedra linked by corners to MO$_6$ octahedra. Each XO$_4$ tetrahedron shares each corner with one MO$_6$ octahedron and conversely, each MO$_6$ octahedron shares each corner with a different XO$_4$ group. The interstitial voids generated within the network are of two types known as M1 and M2 sites (1 : 3 multiplicity). The large charge-compensating Na$^+$ cations are located in these positions. An initial approach to correlate electrical parameters (ionic conductivities and activation energies) with generic average structural parameters (unit cell constants) was followed by scrutiny of specific structural factors such as the size of the bottleneck that connects the M1 and M2 sites.[9] However, to establish possible correlations of this type, full crystal structure information is required. This may be obtained either by single crystal diffraction or by Rietveld analysis of powder diffraction data.[10,11]

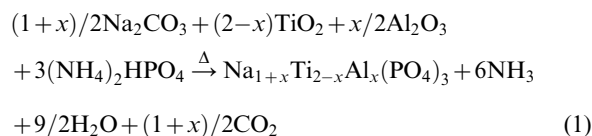On the other hand, there are few reports of NASICON materials containing Al cations. These works mainly deal with lithium based ionic conductors. The small octahedral ionic radius of Al^{3+} is likely in the tolerability limit of the NASICON framework. Furthermore, in the ceramic synthesis of these compounds, ALPO type side-compounds can be easily formed. Phases such as berlinite, with tetrahedral AlO$_4$ groups, are very stable and once formed do not react to yield the desired material. So, well characterised series are lacking but some have been published, e.g. A$_{1+x}$M$^{IV}_{2-x}$Al$_x$(PO$_4$)$_3$ where x_{max} = 0.4, and A = Li[12,13] or Na.[14] One of the reasons for the low Al content in the reported NASICONs, so far, is the conditions of the ceramic syntheses with very high temperatures that result in a mixture of phases.

The aim of this work is to establish the synthetic conditions to enhance the Al content of NASICON materials. We have chosen the Na$_{1+x}$Ti$_{2-x}$Al$_x$(PO$_4$)$_3$ series because of the low cost of the elements, the non harmful nature of the chemicals and the relative similarity of the ionic radii. We have characterised the resulting compounds by different techniques.

Experimental

Synthesis

The materials have been prepared by solid state reaction. Stoichiometric quantities of Na$_2$CO$_3$, activated TiO$_2$, γ-Al$_2$O$_3$ and (NH$_4$)$_2$HPO$_4$ were heated to give the following overall reaction:

$$(1+x)/2\text{Na}_2\text{CO}_3 + (2-x)\text{TiO}_2 + x/2\text{Al}_2\text{O}_3$$

$$+ 3(\text{NH}_4)_2\text{HPO}_4 \xrightarrow{\Delta} \text{Na}_{1+x}\text{Ti}_{2-x}\text{Al}_x(\text{PO}_4)_3 + 6\text{NH}_3$$

$$+ 9/2\text{H}_2\text{O} + (1+x)/2\text{CO}_2 \quad (1)$$

Activated TiO$_2$ was prepared by slow hydrolysis of commercial Ti(OCH(CH$_3$)$_2$)$_4$ with a 1 : 4 water-to-propanol solution. The resulting white suspension was centrifuged, washed thoroughly with water, and heated at 300 °C for 24 h.

DOI: 10.1039/b004837m

Part of this sample was heated at 1000 °C to determine the small weight loss due to hydration residual water. This was taken into account when preparing the stoichiometric reagent mixture.

The synthesis of these materials has been optimised by studying the choice of reagents and heating temperatures, rates and times. The final synthetic procedure is as follows: 1) the reagents were weighted and ground in an agate mortar for 3 h using acetone to help their homogenisation; 2) the mixtures were heated at 0.5 °C min^{-1} up to 400 °C and held at that temperature for 8 h; 3) after 10 min of grinding, a second thermal treatment was carried out at 550 °C for 12 h which resulted in the complete loss of H_2O, NH_3, and CO_2; 4) finally, the mixtures were ground for another 3 h, pelletised and heated at 725 °C for 48 h. The studied compositions were Na_{1+x}-$Ti_{2-x}Al_x(PO_4)_3$ ($x = 0.0, 0.2, 0.4, 0.6, 0.8$ and 0.9).

X-Ray diffraction and thermodiffractometry

X-Ray powder diffraction patterns were collected on a Siemens D5000 automated diffractometer with ($\theta/2\theta$) Bragg–Bretano geometry using graphite monochromated $CuK_{\alpha1,2}$ radiation. The XRD patterns were recorded between 12° and 50° 2θ for indexing purpose and to follow the chemical reactions. Patterns were collected between 14 and 125° (2θ) with 0.03° step size for 14 s (counting time) in order to refine the crystal structures by the Rietveld method.[15] Thermodiffractometric data were recorded with the same diffractometer but in a second goniometer permanently equipped with a HTK10 heating chamber. The patterns were scanned over the angular range 10–38° (2θ), with a step size of 0.04° and counting 1 s per step. A delay time of 10 minutes, before any data acquisition, was selected to ensure sample thermal stabilisation.

Thermal analysis

Thermogravimetric and differential thermal analyses (TG-DTA) were performed for all compositions on a Rigaku Thermoflex TG8110 apparatus. The temperature was varied from RT up to 900 °C at a heating rate of 10 K min^{-1} with calcined Al_2O_3 as reference.

Ionic conductivity

Cylindrical pellets ($\sim$10 mm of diameter and $\sim$1.5 mm thickness) of the samples were obtained by applying a uniaxial pressure of 100 MPa. The pellets were heated at 725 °C for 24 h. The porosity of the pellets, determined from the masses and geometry, ranges between 25 and 10%. Electrodes were made by sputtering of gold on opposite pellet faces. Conductivities were determined, by a.c. impedance measurements from 20 Hz to 1 MHz using a Hewlett-Packard 4284 impedance analyser, at 15 °C intervals on a heating from 233 to 473 K.

Results and discussion

The synthesis study showed that the compositional limit in the $Na_{1+x}Ti_{2-x}Al_x(PO_4)_3$ series is $x_{max} = 0.9$. All attempts to introduce more aluminium resulted in phase separation. The final temperature of the syntheses could not be raised above 900 °C as the materials start to decompose. Very long heating (more than 60 h) at 750 °C also results in partial decomposition.

Lower final temperatures were also tested in order to extend the compositional range to $x > 0.9$. These attempts were also unsuccessful. However, by heating the $x = 0.9$ composition at 550 °C for 24 h, a single phase with a powder pattern similar to those of $R\bar{3}c$ NASICON materials but with many low intensity diffraction peaks was obtained. All peaks were autoindexed in a monoclinic cell using the TREOR90 program. The resulting

parameters were $a = 16.135(4)$ Å, $b = 8.712(1)$ Å, $c = 14.347(3)$ Å and $\beta = 106.60(1)°$ with figures of merit $M_{14} = 22$ and $F_{14} = 23$. Its powder pattern is clearly related to that of the high temperature rhombohedral NASICON compounds but with some type of distortion. However, the low temperature synthesis leads to a compound with low crystallinity, without sharp peaks, that precludes the structure determination from powder diffraction data. A thermodiffractometric study of this materials indicated that it changes to the rhombohedral NASICON structure above 800 °C.

The X-ray diffraction study shows that the samples obtained at 725 °C were polycrystalline phases. The powder patterns could be fully explained by the typical $R\bar{3}c$ NASICON type structure. In some syntheses, a minor side phase, $NaAlP_2O_7$, was detected. The crystal structures of the six phases, $Na_{1+x}Ti_{2-x}Al_x(PO_4)_3$ ($x = 0.0, 0.2, 0.4, 0.6, 0.8, 0.9$), were refined by the Rietveld method[15] using the GSAS suit of programs.[16] The structure of $NaTi_2(PO_4)_3$ was used as a starting model.[10] The nominal Ti/Al composition was randomly distributed in the octahedral site. The extra Na content, to compensate the Ti substitution by Al, was placed in the M2 site. Firstly, the common overall parameters, histogram scale factor, background coefficients, unit-cell parameters, zero-shift, error and pseudo-Voigt coefficients were refined. Then, the positional parameters were optimised. After convergence, the Ti/Al fractions were allowed to vary but constrained to full occupancy. The deviations of the occupation factors from the nominal composition were very small and so, they were fixed to the nominal values. Hence, the occupation factors of Na(2) site were also fixed to the nominal values. Refinements of the Na(1) site occupancy indicated no vacancies for any compositions. Isotropic temperature factors for each site were refined.

The unit cell parameters and the R-agreement Rietveld factors are given in Table 1 for the full series. The weight fractions of the side-phase, $NaAlP_2O_7$, are also given in Table 1 and they do not depend on the composition. The structural parameters are given in Table 2. Selected inter-atomic distances and bond angles are given in Tables 3 and 4, respectively. The powder pattern of $Na_{1.9}Ti_{1.1}Al_{0.9}(PO_4)_3$ is shown in Fig. 1 as an example.

It can be seen in Table 1 that the volume decreases steadily along the series. The ionic radius of Al^{3+} (0.535 Å) is smaller than that of Ti^{4+} (0.605 Å) which explains the volume contraction with Al.[17] However, this cell variation is not isotropic as the a-axis parameters remain almost constant with x and the c-axis parameters markedly decrease along the series. On the basis of the structural data obtained by the Rietveld refinements, the anisotropic contraction can be rationalised as follows. The decrease in c-axis with x is due to a diminution of the average M–O bond distances, Table 3. The intra-lantern P–O(1)–M angles change little from 153.8° for Al_0 to 152.2° for $Al_{0.9}$ and the inter-lantern P–O(2)–M angles do not change appreciably, Table 4 and Fig. 2. Consequently, the M...M intra-lantern and M...M inter-lantern distances [both along the c-axis] decrease along the series. This is different behaviour than that observed in the $Na_{1+x}Zr_{2-x}In_x(PO_4)_3$ series[11] where the contraction of the c-axis took place with a decrease of the M...M intra-lantern distances and an increase of the M...M inter-lantern distances, Fig. 2. This behaviour is explained because In^{3+} is larger than Zr^{4+} and here, Al^{3+} is smaller than Ti^{4+}.

The filling of the M2 sites produces also a modification of their oxygen environment. For Al_0, the M2 sites are vacant and the void is very anisotropic with four long distances to O(1) (2×2.92 Å and 2×2.62 Å) and four shorter distances to O(2) (2×2.24 Å and 2×2.31 Å). As this site is progressively filled, the environment becomes more regular, Table 3, Na(2)–O(1) bond distances become shorter and Na(2)–O(2) distances larger. For $Al_{0.9}$, the distances are 2×2.80 Å and 2×2.58 Å for O(1) and 2×2.38 Å and 2×2.29 Å for O(2). The main

Table 1 Crystallographic parameters for $Na_{1+x}Ti_{2-x}Al_x(PO_4)_3$ and side-phase content, $NaAlP_2O_7$, from Rietveld studies

x	$a/Å$	$c/Å$	$V/Å^3$	R_{wp} (%)	R_p (%)	χ^2	R_F (%)	% w/w $NaAlP_2O_7$
0.0	8.4627(4)	21.935(1)	1360.5(2)	14.72	10.75	1.94	3.3	—
0.2	8.4824(2)	21.7762(8)	1356.9(1)	14.40	10.38	2.25	3.1	2.58(2)
0.4	8.4825(1)	21.7315(6)	1354.2(1)	12.56	8.90	1.78	2.6	5.68(2)
0.6	8.4825(1)	21.6691(6)	1350.3(1)	12.48	9.06	1.84	2.8	4.80(2)
0.8	8.4820(2)	21.6187(7)	1347.0(1)	13.10	9.37	2.05	3.3	2.03(2)
0.9	8.4846(1)	21.5994(6)	1346.6(1)	12.98	9.13	2.07	3.4	—

Table 2 Refined structural parameters for $Na_{1+x}Ti_{2-x}Al_x(PO_4)_3$ series

		Al_0	$Al_{0.2}$	$Al_{0.4}$	$Al_{0.6}$	$Al_{0.8}$	$Al_{0.9}$
Na(2) (18e)[a]	x	—	0.590(7)	0.616(3)	0.627(2)	0.626(2)	0.631(1)
Na(1) (6b)[a]	$U_{iso}\times 100$	3.5(3)	2.4(2)	3.1(2)	4.4(2)	4.7(2)	5.4(2)
Ti-Al (12c)[b]	z	0.1453(1)	0.1450(1)	0.1452(1)	0.1453(1)	0.1458(1)	0.1456(1)
(0 0 z)	$U_{iso}\times 100$	−0.02(8)	−0.04(6)	0.00(5)	0.27(5)	0.02(8)	0.23(5)
P (18e)	x	0.2891(4)	0.2877(3)	0.2876(2)	0.2878(2)	0.2876(3)	0.2877(2)
(x 0 1/4)	$U_{iso}\times 100$	1.0(1)	0.23(7)	0.43(6)	0.61(6)	0.6(1)	0.68(6)
O(1) (36f)	x	0.1724(7)	0.1752(5)	0.1739(4)	0.1724(4)	0.1723(5)	0.1717(4)
(x y z)	y	−0.0298(8)	−0.0256(6)	−0.0277(5)	−0.0283(5)	−0.0298(6)	−0.0293(5)
	z	0.1932(3)	0.1929(2)	0.1923(2)	0.1918(1)	0.1913(2)	0.1915(1)
	$U_{iso}\times 100$	0.1(2)	0.9(1)	1.0(1)	1.0(1)	0.9(2)	1.0(1)
O(2) (36f)	x	0.1922(6)	0.1899(4)	0.1907(4)	0.1908(3)	0.1906(5)	0.1901(4)
(x y z)	y	0.1637(6)	0.1621(5)	0.1639(4)	0.1642(4)	0.1645(5)	0.1640(4)
	z	0.0890(3)	0.0881(2)	0.0878(2)	0.0885(2)	0.0885(2)	0.0889(2)
	$U_{iso}\times 100$	0.2(2)	0.1(1)	0.2(1)	0.4(1)	0.2(1)	0.2(1)

[a]U_{iso} of both sodium sites were refined constrained to have the same value. [b]Ti/Al occupation factors fixed to the nominal composition.

structural change produced along the series is the movement of O(1) towards the M2. This results in an slight opening of the O(1)–M–O(1) angles and a small closing of the P–O(1)–M angles, Table 4 and Fig. 2. The more important degree of freedom, which adjusts along with the incorporation of Na on the M2 site, is the flexibility of the MO_6 octahedra which distort by opening the O(1) face thus allowing these oxygens to

move towards Na(2). This O(1) movement counteracts the M–O bond decrease which results in a very small variation of the a-axis along the series. For $Na_{1+x}Zr_{2-x}In_x(PO_4)_3$ series[11] the same mechanism took place, but as In^{3+} is larger than Zr^{4+} the O(1) movement was not counteracted and a large a-axis increase was measured.

The thermal study by TG-DTA shows no weight loss

Table 3 Selected inter-atomic distances for $Na_{1+x}Ti_{2-x}Al_x(PO_4)_3$ series

	Al_0	$Al_{0.2}$	$Al_{0.4}$	$Al_{0.6}$	$Al_{0.8}$	$Al_{0.9}$	Δ (%)[a]
M–O(1)×3	1.914(5)	1.914(4)	1.905(3)	1.887(3)	1.881(4)	1.879(3)	−1.8
M–O(2)×3	1.960(5)	1.951(4)	1.963(3)	1.955(3)	1.959(4)	1.948(3)	−0.6
P–O(1)×2	1.530(5)	1.516(4)	1.526(4)	1.539(3)	1.543(4)	1.543(3)	+0.8
P–O(2)×2	1.511(4)	1.537(4)	1.527(3)	1.526(3)	1.526(3)	1.531(3)	+1.3
Na(1)–O(2)×6	2.474(5)	2.440(4)	2.438(3)	2.446(3)	2.443(4)	2.446(3)	−1.1
Na(2)–O(1)×2	2.92[b]	3.09(5)	2.90(2)	2.83(1)	2.83(1)	2.80(1)	−4.1
Na(2)–O(1)×2	2.62[b]	2.580(5)	2.584(5)	2.588(4)	2.568(5)	2.582(4)	−1.4
Na(2)–O(2)×2	2.24[b]	2.11(5)	2.28(2)	2.36(1)	2.34(1)	2.38(1)	+6.2
Na(2)–O(2)×2	2.31[b]	2.363(18)	2.314(6)	2.296(4)	2.302(5)	2.293(3)	−0.7
Na(1)...Na(2)×6	3.190(1)	3.142(15)	3.200(8)	3.229(6)	3.222(6)	3.237(5)	+1.5
Na(2)...Na(2)×4	4.528(1)	4.442(31)	4.571(16)	4.636(13)	4.627(13)	4.660(9)	+2.9
Na(2)...Na(2)×4	4.494(1)	4.444(10)	4.481(6)	4.495(4)	4.485(4)	4.494(3)	+0.0
M...M[c]	4.591(6)	4.573(4)	4.555(4)	4.535(4)	4.506(6)	4.509(4)	−1.8
M...M[d]	6.377(6)	6.315(4)	6.311(4)	6.299(4)	6.303(6)	6.291(4)	−1.3

[a]Relative increase $= 100\times(Y_x - Y_0)/Y_0$. [b]Calc. distances for an imaginary atom at (0.61 0 ¼) position. [c]Intra-lantern distance [along c-axis]. [d]Inter-lantern distance [along c-axis].

Table 4 Selected bond angles for $Na_{1+x}Ti_{2-x}Al_x(PO_4)_3$ series

|	Al_0	$Al_{0.2}$	$Al_{0.4}$	$Al_{0.6}$	$Al_{0.8}$	$Al_{0.9}$	Δ (%)
P–O(1)–M	153.8(4)	154.1(3)	153.0(2)	152.8(2)	151.6(3)	152.2(2)	−1.0
P–O(2)–M	145.5(4)	144.3(3)	144.2(2)	145.1(2)	145.0(3)	145.5(2)	+0.0
O(1)–M–O(1)×3	92.8(3)	93.1(2)	93.8(1)	94.2(1)	95.1(2)	94.7(1)	+2.0
O(1)–M–O(2)×3	91.2(2)	90.7(1)	90.8(1)	90.5(1)	90.4(1)	90.4(1)	−0.9
O(1)–M–O(2)×3	174.2(3)	173.5(2)	173.1(2)	173.2(2)	172.4(3)	172.8(2)	−0.8
O(1)–M–O(2)×3	91.3(2)	91.9(2)	91.0(1)	90.4(1)	89.7(2)	89.8(1)	−1.6
O(2)–M–O(2)×3	84.4(3)	84.0(2)	84.0(2)	84.5(1)	84.3(2)	84.6(2)	+0.2
O(1)–P–O(1)	111.4(5)	112.2(4)	112.6(3)	112.2(3)	113.0(4)	112.3(3)	+0.8
O(1)–P–O(2)×2	105.5(3)	105.8(2)	105.3(2)	105.7(2)	105.3(2)	105.8(2)	+0.3
O(1)–P–O(2)×2	111.6(2)	111.4(2)	112.1(2)	111.2(2)	111.9(2)	111.8(2)	+0.2
O(2)–P–O(2)	111.5(5)	110.4(4)	109.6(3)	109.7(3)	109.4(4)	109.5(3)	−1.8
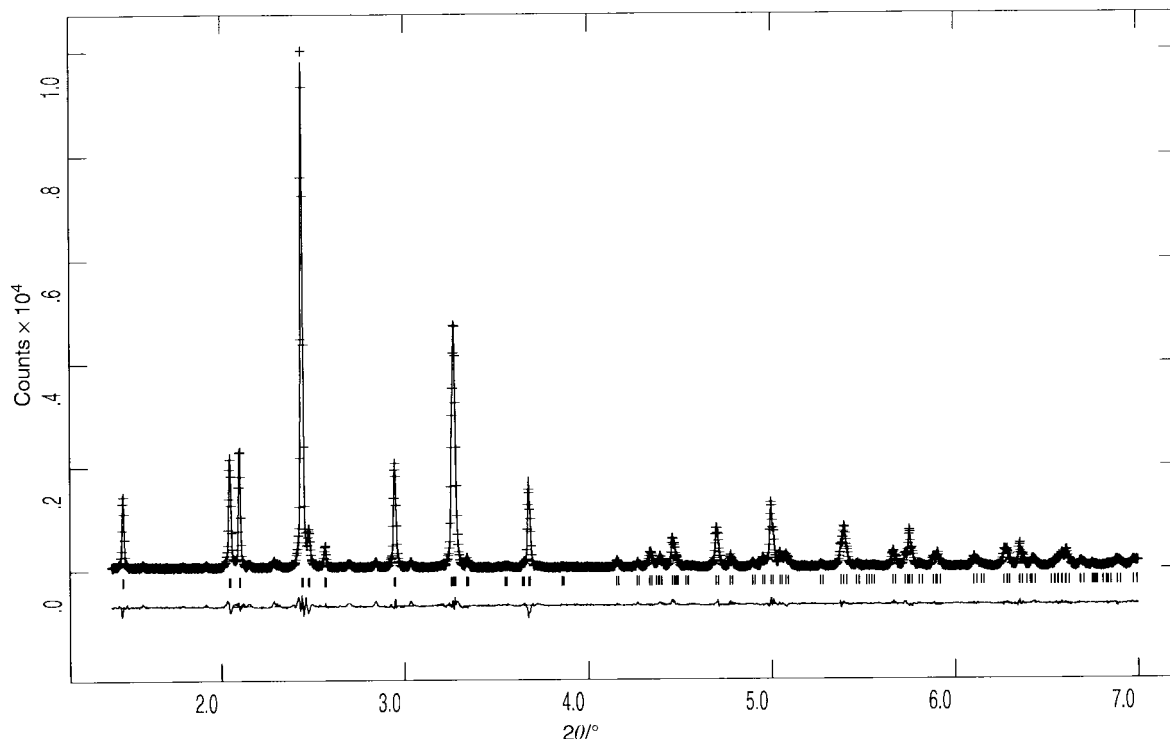
Fig. 1 Observed, calculated and difference laboratory X-ray diffraction patterns for $Na_{1.9}Ti_{1.1}Al_{0.9}(PO_4)_3$.

between room temperature and 900 °C for all compositions. Endotherms were not observed for $x < 0.8$ compositions in the DTA curves. However, a small endothermic effect was observed for $x = 0.8$ and 0.9 compositions near to 725 °C. A thermodiffractometric study for $Na_{1.8}Ti_{1.2}Al_{0.8}(PO_4)_3$ was undertaken to characterise this effect. The powder patterns showed no phase transition and only the peaks displacement due to the thermal expansion was observed. The cell parameters were obtained by Rietveld refinement of the variable-T patterns. A slight linear contraction of the a-axis parameter and a small linear expansion of the c-axis coefficient is observed, Fig. 3. The thermal expansion coefficients deduced from these data were $\alpha_a = -2.4 \times 10^{-6} K^{-1}$, $\alpha_c = +23 \times 10^{-6} K^{-1}$ and $\alpha_V = +16 \times 10^{-6} K^{-1}$. This anisotropic thermal behaviour is typical of the anisotropic NASICON framework and it is due to the thermal behaviour of rigid PO_4 tetrahedra and more flexible MO_6 octahedra. Hence, the observed endotherms are probably not due to a phase transition. If a transition takes place, the associated structural changes have to be very small since no changes are detected in the powder

patterns. More likely, these endotherms may be due to the reaction of amorphous unreacted compounds.

Some results from the impedance study of $Na_{1.8}Ti_{1.2}Al_{0.8}(PO_4)_3$ are shown in Fig. 4, 5 and 6. These data are typical for all compositions and they allow one to characterise the electrical properties of these samples. The complex impedance plane plot, Fig. 4, shows that these pellets are ionic conductors. At high temperatures, for example 473 K, the spike due to the blocking electrode effect is clearly shown at the lowest frequencies, see inset of Fig. 4. At lower temperatures, i.e. 350 K, this plot points out a set of high frequency overlapped semicircles. This set of semicircles indicates that
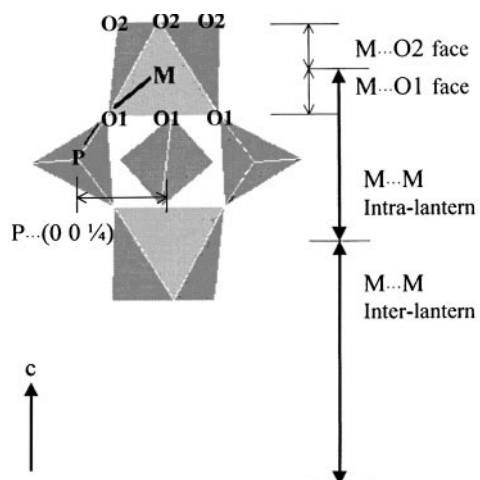

Fig. 2 (010) view of the simplest NASICON structural motif (lantern unit) showing the atom labelling and selected distances.
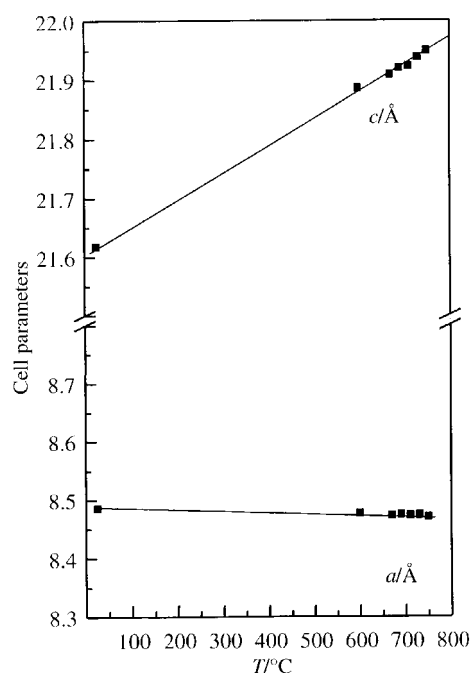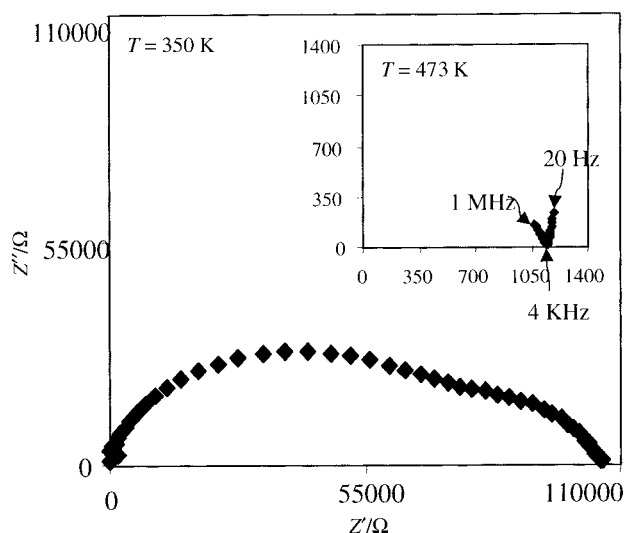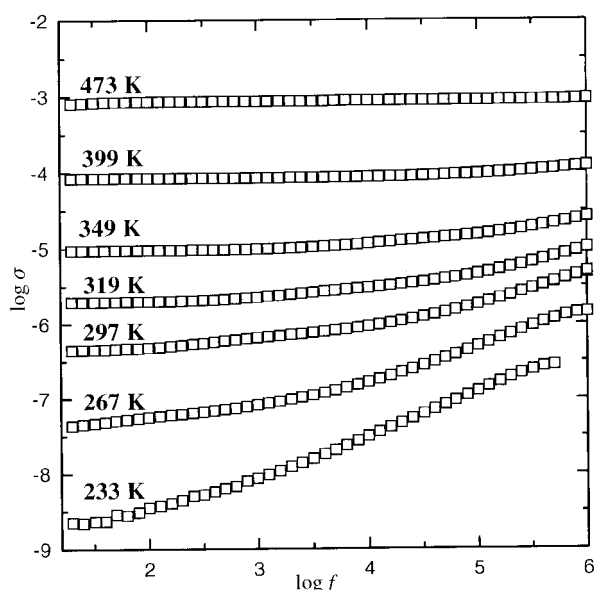

Fig. 3 Variation of lattice parameters with temperature for $Na_{1.8}Ti_{1.2}Al_{0.8}(PO_4)_3$.
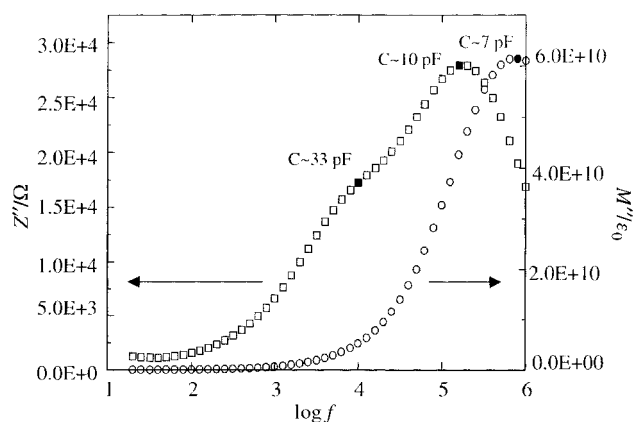
Fig. 4 Complex impedance plane plot at 350 K (473 K in the inset) for $Na_{1.8}Ti_{1.2}Al_{0.8}(PO_4)_3$.

Fig. 5 Real part of the conductance *vs.* log of frequency at several selected temperatures for $Na_{1.8}Ti_{1.2}Al_{0.8}(PO_4)_3$.

Fig. 6 Spectroscopic plots for $Na_{1.8}Ti_{1.2}Al_{0.8}(PO_4)_3$ at 350 K: Impedance imaginary part, Z'', and complex electric modulus, M'', versus $\log f$.

Table 5 Ionic conductivities and activation energies for $Na_{1+x}Ti_{2-x}Al_x(PO_4)_3$

| x	Pellet porosity (%)	$\sigma_{100\,°C}$/S cm^{-1}	$\sigma_{25\,°C}$/S cm^{-1}	E_{ac}/eV
0.4	25	3.5×10^{-6}	5.6×10^{-8}	0.54
0.6	22	5.9×10^{-6}	1.1×10^{-7}	0.56
0.8	12	7.0×10^{-6}	1.2×10^{-7}	0.55
0.9	10	7.2×10^{-6}	1.3×10^{-7}	0.51

several effects are involved in the electrical response of the pellets, including bulk and grain-boundary contributions.

Fig. 5 shows conductivity data in the frequency range 20 Hz–1 MHz at several temperatures for $Na_{1.8}Ti_{1.2}Al_{0.8}(PO_4)_3$ which is representative of the behaviour of the series. The absence of a clear plateau at intermediate frequencies rules out the possibility of extracting the bulk conductivities values. This is due to the similar nature of the conductivity of the grain boundary and in the bulk of the grains. This thermal behaviour is typical of poor sintered ionic conductors.

A deeper insight into the electrical microstructure of the pellets can be obtained from the spectroscopic plots of the impedance imaginary part, Z'', and the complex electric modulus, M''. These plots are shown in Fig. 6 for $Na_{1.8}Ti_{1.2}Al_{0.8}(PO_4)_3$ at 350 K. The Z'' plot shows a broad peak with a pronounced shoulder at lower frequencies and the M'' plot a broad single peak. The capacitances of selected points in this graph are also shown. The maxima of both curves are separated by about one decade in frequency. Hence, these maxima are associated with the bulk/intrinsic response of the sample. The shoulder in the overall Z'' plot, with an associated capacitance of ~ 33 pF, is very likely due to a grain-boundary impedance. Because its capacitance is quite high it is not readily seen in the M'' spectrum, but it makes an important contribution to the overall pellet impedance. This complex response is mainly due to the poor sintering of the pellets. This is a consequence of the thermal stability of the material as it can not be heated above 800 °C without partial decomposition. The porosity of the pellets decreases as the Al content increases, see Table 5.

The non-conventional Arrhenius plots, where the logarithm of the frequency maxima of the M'' signal is represented *versus* $1000/T$, are shown in Fig. 7. The activation energies, as deduced from the slopes of Arrhenius representations, are also given in Table 5. The activation energies do not change appreciably along the series. Overall conductivity data directly extracted from the complex impedance plane plot are given in
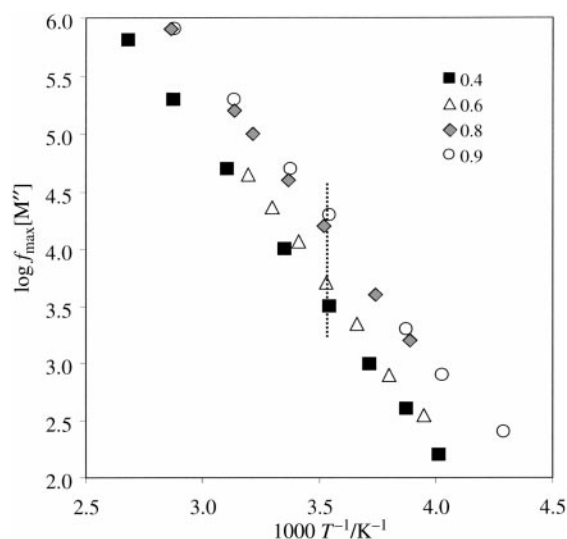
Fig. 7 Variation of log $f_{max}[M'']$ *versus* $1000/T$ for $Na_{1+x}Ti_{2-x}Al_x(PO_4)_3$ ($x = 0.4$, 0.6, 0.8, 0.9).

Table 5. The overall conductivities increase with x but it is hard to discuss this variation as the porosities and grain-boundary contributions are different along the series. However, the Arrhenius lines from the M'' data fall on a set of spaced parallel lines, Fig. 7, showing a clear trend of increasing *bulk conductivity* with x.

Conclusions

The $Na_{1+x}Ti_{2-x}Al_x(PO_4)_3$ solid solution has been prepared and the compositional limit was determined. The diffracto-metric study showed that these compounds crystallise in the $R\bar{3}c$ NASICON type structure and the structural changes along the series have been elucidated. These compounds have the highest Al content in a NASICON series reported so far. They display low anisotropic thermal expansion that was measured by powder thermodiffractometry. The ionic conductivities of Na^+ are low as is expected in a NASICON framework built up by small octahedral metals. The resulting bottleneck sizes are small for Na^+ hopping but it may be suitable for the Li^+ cations. We are preparing Li derivatives by ion-exchange to test this hypothesis.

Acknowledgements

References

1　H. Y-P. Hong, *Mater. Res. Bull.*, 1976, **11**, 173.
2　J. B. Goodenough, H. Y-P. Hong and J. A. Kafalas, *Mater. Res. Bull.*, 1976, **11**, 203.
3　Y. Saito, K. Ado, T. Asai and O. Nakamura, *J. Mater. Sci. Lett.*, 1992, **11**, 888.
4　C. Delmas, A. Nadiri and J. L. Soubeyroux, *Solid State Ionics*, 1988, **28-30**, 419.
5　J. M. Winand, A. Rulmont and P. Tarte, *J. Solid State Chem.*, 1991, **93**, 341.
6　S. Hamedoune, M. Gondrand and D. Tran Qui, *Mater. Res. Bull.*, 1986, **21**, 237.
7　H. Aono, E. Sugimoto, Y. Sadaoka, N. Imanaka and G. Adachi, *Chem. Lett.*, 1990, 1825.
8　M. Sugantha, U. V. Varadaraju and G. V. Subba Rao, *J. Solid State Chem.*, 1994, **111**, 33.
9　H. Kholer and H. Schulz, *Mater. Res. Bull.*, 1986, **21**, 23; H. Kholer and H. Schulz, *Mater. Res. Bull.*, 1985, **20**, 1461; H. Kholer and H. Schulz, *Solid State Ionics*, 1983, **9–10**, 795.
10　E. R. Losilla, M. A. G. Aranda, S. Bruque, M. A. Paris, J. Sanz and A. R. West, *Chem. Mater.*, 1998, **10**, 665.
11　E. R. Losilla, M. A. G. Aranda, S. Bruque, M. A. Paris, J. Sanz, J. Campo and A. R. West, *Chem. Mater.*, 2000, **12**, 2134.
12　H. Aono, E. Sugimoto, Y. Sadaoka, N. Imanaka and G. Adachi, *J. Electrochem. Soc.*, 1989, **136**, 590; H. Aono, E. Sugimoto, Y. Sadaoka, N. Imanaka and G. Adachi, *Chem. Lett.*, 1990, 1825; H. Aono, E. Sugimoto, Y. Sadaoka, N. Imanaka and G. Adachi, *J. Electrochem. Soc.*, 1990, **137**, 1023; H. Aono, E. Sugimoto, Y. Sadaoka, N. Imanaka and G. Adachi, *Bull. Chem. Soc. Jpn.*, 1992, **65**, 2200; H. Aono, E. Sugimoto, Y. Sadaoka, N. Imanaka and G. Adachi, *Solid State Ionics*, 1993, **62**, 309.
13　S-C Li, J-Y Cai and Z-X Lin, *Solid State Ionics*, 1988, **28-30**, 1265.
14　J. M. Winand, A. Rulmond and P. Tarte, *J. Mater. Sci.*, 1990, **25**, 4008.
15　H. M. Rietveld, *J. Appl. Crystallogr.*, 1969, **2**, 65.
16　A. C. Larson and R. B. von Dreele, GSAS program, Los Alamos National Lab. Rep. No. LA-UR-86-748, 1994.
17　R. D. Shannon, *Acta Crystallogr., Sect. A*, 1976, **32**, 751.